Decision support to conceive optimized transparent transpired collectors (TTC)

Guy Clarence Sèmassou, Victorin Chegnimonhan, Henri Hounkpatin, Antoine Vianou & Gérard Degan

International Journal on Interactive Design and Manufacturing (IJIDeM)

ISSN 1955-2513

Int J Interact Des Manuf
DOI 10.1007/s12008-016-0348-x

Springer

Int J Interact Des Manuf
DOI 10.1007/s12008-016-0348-x

ORIGINAL PAPER

Decision support to conceive optimized transparent transpired collectors (TTC)

Guy Clarence Sèmassou[1,3] · Victorin Chegnimonhan[2] · Henri Hounkpatin[1] · Antoine Vianou[3] · Gérard Degan[1]

Received: 22 July 2016 / Accepted: 22 August 2016

Abstract This research work focuses on the preconception and optimization of transparent transpired collectors (TTC) for preheating air in buildings. To achieve this objective, a theoretical approach based on the developed physical model was adopted to simulate the behaviour of TTC. The daily time evolution of the intrinsic parameters of the concerned solar collector are evaluated in order to analyse their impact on the performance of TTC. The optimization was carried out through the variation of the design geometrical parameters such as pitch diameter and pitch holes to maximize both the collector energyefficiency and the recovered heat rate, and this way, minimizing the temperature difference between the incoming air and the outgoing one. To reach the goal, desirability functions have been defined and implemented for the search of the optimum candidates of design parameters. In the context of our study case, an optimized pair of design variables (holes diameter and pitch) is proposed.

✉ Guy Clarence Sèmassou
seclar2001@yahoo.fr

Victorin Chegnimonhan
victorin.chegnimonhan@gmail.com

Antoine Vianou
avianou@yahoo.fr

1 Laboratoire d'Energétique et de Mécanique Appliquée (LEMA), Université d'Abomey-Calavi, 01 BP 2009, Cotonou, Benin

2 Laboratoire de Thermocinétique(LTN), CNRS UMR 6604, Université de Nantes, La Chantrerie, Nantes, France

3 Laboratoire de Caractérisation Thermophysique des Matériaux et d'Appropriation Energétique (LABO-C. T. M. A. E.), Universitéd'Abomey-Calavi, 01 BP 2009, Cotonou, Benin

Keywords Transparent transpired collector · Solar energy · Solar wall · Heat transfer · Conception · Optimization

Nomenclature

A_T	Total collector area (m^2)
ALC	Absolute lower cutoff
AUC	Absolute upper cutoff
$C_{\bar{p},in}$	Specific heat of air coming out of plate and entering the plenum (J/kg K)
$C_{\bar{p},out}$	Exit air specific heat of plenum (J/kg K)
D	Perforation diameter (m)
d	Desirability
d_{plen}	Plenum depth (m)
G_{Sol}	Incident solar radiation (W/m^2)
H	Collector height (m)
K_{air}	Thermal conductivity of air (W/m K)
LSL	Lower soft limit
$\dot{m}_{amb}$	Mass flow rate of air through the collector (kg/s)
$\dot{m}_{in}$	Mass flow rate from perforated plate to plenum (kg/s)
$\dot{m}_{out}$	Exit air mass flow of plenum (kg/s)
OF	Global desirability function
P	Pitch of perforations (m)
Pr_w	Prandtl number on wall
$q_{cond,w}$	Transfer by conduction of wall with inside the building (W)
$q_{conv,out}$	Exit convective transfer of collector (W)

Greek symbols

$\alpha_{eff,p}$	Effective absorptivity of plate
α_p	Absorptivity of plate

Published online: 30 August 2016

α_T	Thermal diffusivity (m^2/s)
α_w	Absorptivity of wall
ΔT	Temperature difference (K)
$\varepsilon_{eff,p-amb}$	Effective emissivity between the plate and the ambient
$\varepsilon_{eff,p-w}$	Effective emissivity between the plate and the wall
ε_p	Emissivity of plate
ε_w	Emissivity of wall
$q_{conv,p-amb}$	Convection heat transfer from air to plate (W)
$q_{conv,p-plen}$	Transfer by convection of outgoing plate and entering the plenum (W)
$q_{conv,p-amb}$	Convection heat transfer from air to plate (W)
$q_{conv,p-plen}$	Transfer by convection of outgoing plate and entering the plenum (W)
$q_{conv,p-loss}$	Convective losses between the plate and the ambient (W)
$q_{conv,w-plen}$	Convective transfer from wall to air plenum (W)
q_{out}	Net rate of heat recovered (J)
$q_{rad,Sol-p}$	Solar radiation absorbed by the semi-transparent plate (W)
$q_{rad,Sol-w}$	Solar radiative transfer absorbed by the wall (W)
$q_{rad,p-amb}$	Net radiative transfer between the plate and the ambient (W)
$q_{rad,w-p}$	Radiative transfer from the wall to plate (W)
Re_w	Reynolds number on wall
T_{amb}	Ambient air temperature
T_{int}	Air temperature leaving the perforated plate and entering the plenum (K)
T_{out}	Exit air temperature of plenum (K)
T_p	Temperature of plate (K)
T_w	Temperature of wall (K)
USL	Upper soft limit for the criterion
w_n	Weights
Y_m	Criterion
η	Efficiency collector
ρ_{air}	Density of air (kg/m^3)
ρ_p	Reflectivity of plate
ρ_w	Reflectivity of wall
$\widehat{\sigma}$	Stephan Boltzmann Constant (5.67×10^{-8} $Wm^{-2}K^{-4}$)
ν_{plen}	Kinematic viscosity (m^2/s)
μ_{air}	Dynamic viscosity of air (kg/ms)
τ_p	Transmissivity of plate

1 Introduction

For decades, energy consumption is growing strongly worldwide. It's obvious that energy needs will continue to increase as a result of economic growth and increase in per capita electricity consumption [1]. Thus, considering just the decade 2001–2011, world energy consumption increased from 9.434 million tons of oil equivalent (Mtoe) to 12,275 Mtoe, meaning a growth of almost 23 % [2]. The concern of depletion of the global fossil fuel reserves (oil, coal, gas, etc.), and the global economic crisis (oil price rises), or the accidents of nuclear power plants such as those at Three Mile Island (USA 1979), Chernobyl (USSR 1986) and Fukushima (Japan 2011) [3], moreover the concern for pollution strengthens the interest of the general public towards renewable energy [3]. The sustainable resource of interest in this study is the solar energy for thermal engineering applications. Among the most popular technologies to recover the active solar energy in the building, a focus is made on the "solar walls" in order to preheat inlet fresh air in buildings. One such type of common solar wall is opaque (Unglazed Transpired Collector: UTC). For this configuration, the sun heats the outer perforated plate made of metal coated sheet with a paint that absorbs solar radiation. Thus, the air in contact with the plate is heated and an airflow is induced through the perforations. The other type of solar wall has a perforated transparent outer plate (Transparent Transpired Collector: TTC) and the solar energy is absorbed by the back wall. Unlike UTC which is used for decades, TTC is a proven solar technology, but still emerging. The literature presents interesting research works on the topic. We may mention for example the work of Semenou et al. [4] that presented a simple but effective mathematical model for a solar collector perforated glazing (TTC) with double aspiration to remove the problems of stagnation in the plenum and ensure better thermal efficiency and heat recovery. In his thesis, Badache [5] evaluated the influence of some parameters (the thickness of the plenum, the pitch between the slots, the slot width, mass flow, and the incident solar radiation), including interactions on the performance of a TTC. A first description of the physical phenomena existing in TTC, and a formulation of these by heat balances have been investigated elsewhere [6]. However, the various phenomena studied in the above cited works have been investigated with constant value of the irradiation. But the latter does vary with time. Then the peculiarity of this work is to study and analyse on the TTC the time evolution of some performance criteria as the efficiency, the temperature difference and the net rate of there covered heat in variable irradiation conditions. Furthermore the aim is to find the optimal combinations of design parameters such as diameter and pitch of the holes, which at the same time maximize the performance of the collector and minimize the temperature difference between the incoming air and the outgoing air (a collector is more efficient when

Fig. 1 Scheme of a TTC

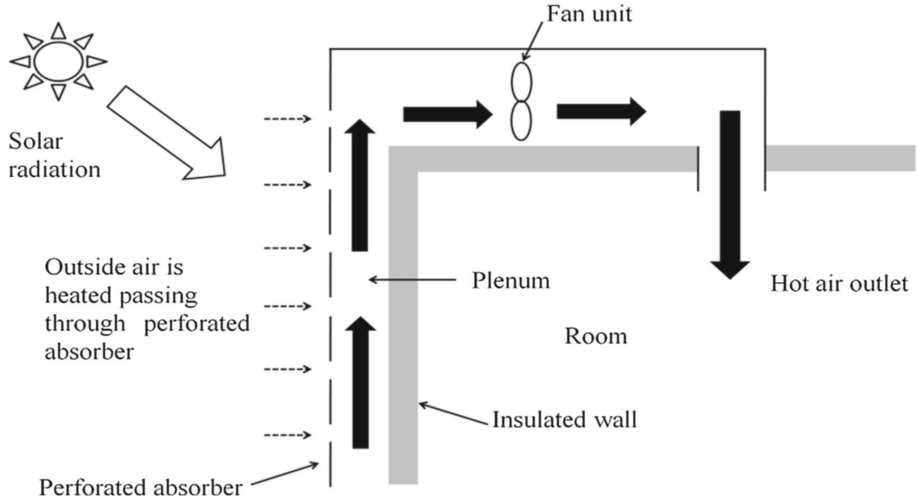

operated at a temperature close to ambient temperature) and implicitly to maximize the rate of heat recovered.

2 Materials and methods

2.1 Collector configuration

The configuration of the TTC is available in Fig. 1. This type of collector is composed of a transparent perforated plate mounted vertically on a wall. The perforated glazing consists of polycarbonate that is a well-known glazing material for solar collectors [5]. Part of the radiation is absorbed by the plate depending on its optical properties. Thus, the wall behind the plate in turn receives a part of the solar radiation and gets heated then. The air ascending through the plenum becomes hotter in contact with the wall. Then the warmed air is blown into the building by a fan.

2.2 Assumptions

The following assumptions are made in TTC modelling:

1. Considering the phenomenon of convection between the semi-transparent plate and the air passing through, the transparent plate behaves like the UTC. The fact that the thickness of plate and the conductivity there are of very little influence on the effectiveness of UTC [6] confirms the validity of this hypothesis;
2. Heat exchange by convection is considered to be identical over the entire surface of the collector. This assumption is required for a first approach and was found to be realistic according to [7];
3. The suction of air and flow phenomena through the transparent plate and into the plenum are considered be identical to those of UTC [1];
4. Heat loss by convection between the plate and the environment is neglected, as observed for UTC [6]. Since the plate of a TTC is semi-transparent, its absorptivity is lower than the one of an UTC, therefore its temperature will necessarily be lower than that of an UTC in the same conditions. Such assumption has been adopted in [1];
5. The air flow rate through the plate is assumed to be constant and homogeneous over the entire perforated plate;
6. The flow is driven from outside to the plenum through the perforated plate then out of it towards the outlet of the collector without any risk of flow reversal.

2.3 Energy balance equations

The different transfer modes governing the operation of TTC are illustrated in Figs. 2 and 3 in order to predict its thermal performance. The balance equations are established respectively for the semi-transparent perforated plate, the plenum, the wall and the collector.

2.3.1 Transparent perforated plate

Figure 2a summarizes the thermal flux exchange at the plate. The equation expressing the different transfers present only the net radiation balance to simplify schemes and for easy insights in equations. Thus, the energy balance on the plaque can be written as follows:

$$q_{rad,Sol-p} - q_{rad,p-w} - q_{rad,p-amb} + q_{conv,p-amb} - q_{conv,p-loss} - q_{conv,p-plen} = 0 \quad (1)$$

The expressions of the terms defined in the energy balance written on the plate are:

$$q_{rad,Sol-p} = \alpha_{eff,p} A_T G_{Sol} \quad (2)$$

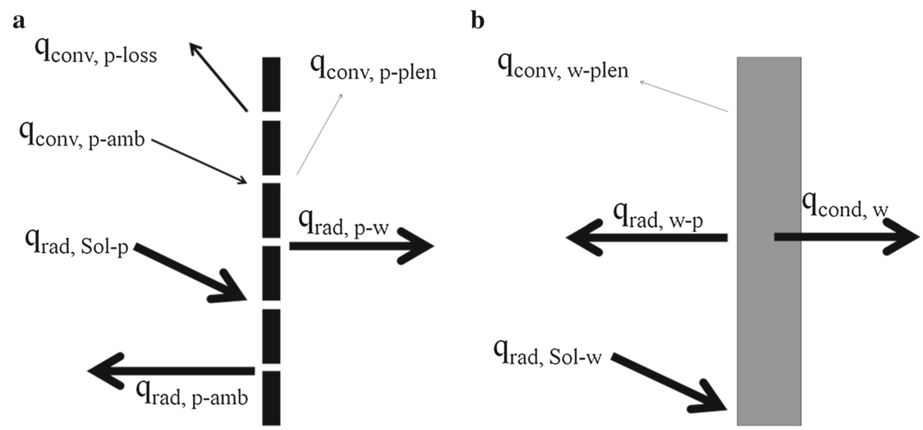

Fig. 2 Heat balance: **a** On the transparent perforated plate and **b** on the wall

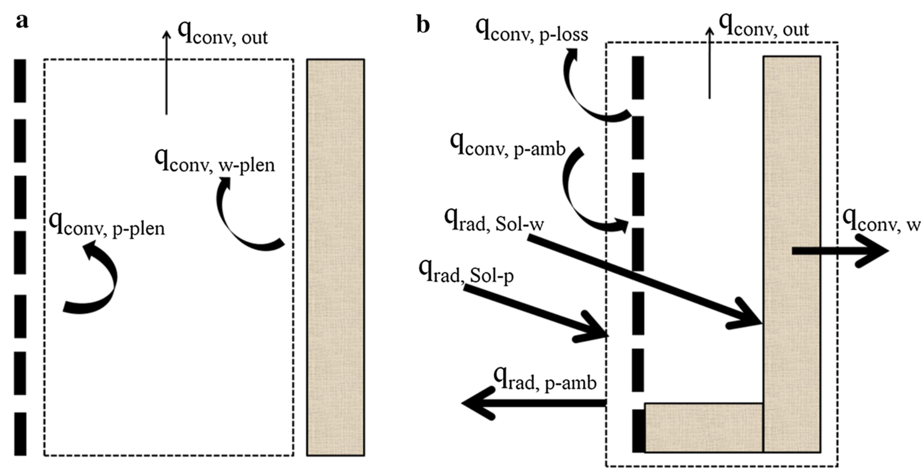

Fig. 3 Heat balance: **a** Balance on the airflow passing through the plenum. **b** Global balance on the collector

Where,

$$\alpha_{eff,p} = \alpha_p + \alpha_p \tau_p \rho_w \frac{1}{1-\rho_w \rho_p} \quad (3)$$

$$q_{rad,p-w} = \varepsilon_{eff,p-w} \tilde{\sigma} A_T \left(T_p^4 - T_w^4\right) \quad (4)$$

Where

$$\varepsilon_{eff,p-w} = 1/\left((1/\varepsilon_w + 1/\varepsilon_p) - 1\right) \quad (5)$$

$$q_{rad,p-amb} = \varepsilon_{eff,p-amb} \tilde{\sigma} A_T \left(T_p^4 - T_{amb}^4\right) \quad (6)$$

The perforated plate is directly exposed to the environment which is considered as a black surface. The shape factor between the plate and the environment is therefore 1 and the effective emissivity between the plate and the environment becomes:

$$\varepsilon_{eff,p-amb} = \varepsilon_p \quad (7)$$

$$q_{conv,p-amb} = \dot{m}_{amb} c_{\bar{p},amb} T_{amb} \quad (8)$$

$$q_{conv,p-plen} = \dot{m}_{in} c_{\bar{p},in} T_{in} \quad (9)$$

$$q_{conv,p-loss} = 0, \ \text{(Assumption)}. \quad (10)$$

Thus, on the plate the heat balance writes:

$$\alpha_{eff,p} A G_{Sol} - \varepsilon_{eff,w-p} \tilde{\sigma} A_T \left(T_p^4 - T_w^4\right) - \varepsilon_{eff,p-amb} \tilde{\sigma} A_T \left(T_p^4 - T_{amb}^4\right) - \dot{m}_{in} \left(c_{\bar{p},in} T_{in} - c_{\bar{p},amb} T_{amb}\right) = 0 \quad (11)$$

2.3.2 Energy balance on the wall

On Fig. 2b are displayed the different heat exchanges at the wall. The heat balance can then be expressed as follows:

$$q_{rad,Sol-w} - q_{conv,w-plen} - q_{rad,w-p} - q_{cond,w} = 0 \quad (12)$$

The empirical correlation reported by [7] can be adopted in this model to estimate the Nusselt number. So, the Nusselt number for the convective heat transfer between the plenum air and the wall is:

$$Nu_w = 0.664 * (\text{Re}_w)^{0.5} * (\text{Pr}_w)^{0.333} \quad (13)$$

where

$$\mathrm{Re}_w = \left(\rho_{air} * \nu_{plen} * H\right) / \mu_{air} \tag{14}$$

$$\mathrm{Pr}_w = \left(c_{\bar{p},in} * \mu_{air}\right) / K_{air} \tag{15}$$

The convective heat transfer coefficient between the plenum air and the wall is estimated from

$$h_w = \left(Nu_w * K_{air}\right) / d_{plen} \tag{16}$$

The different terms involved into the Eq. (9) are expressed as follow:

$$q_{rad,Sol-w} = \alpha_{eff,w} A_T G_{Sol} \tag{17}$$

$$q_{conv,w-plen} = h_w A_T \left(T_w - T_{plen}\right) \tag{18}$$

$$q_{rad,w-p} = \varepsilon_{eff,w-p}\, \tilde{\sigma} A_T \left(T_w^4 - T_p^4\right) \tag{19}$$

It's assumed that:

$$q_{cond,w} = 0 \tag{20}$$

And

$$\varepsilon_{eff,w} = \alpha_w \tau_p / \left(1 - \rho_w \rho_p\right) \tag{21}$$

The energy balance around the wall is written:

$$\varepsilon_{eff,w} A_T G_{Sol} - h_w A_T \left(T_w - T_{plen}\right) - \varepsilon_{eff,w-p} \tilde{\sigma} A_T \left(T_w^4 - T_p^4\right) = 0 \tag{22}$$

2.3.3 Plenum air

Referring to the Fig. 3a, the energy balance around the plenum is:

$$q_{conv,p-plen} + q_{conv,w-plen} - q_{conv,out} = 0 \tag{23}$$

The terms involved in the Eq. (23) can be expressed as follow:

$$q_{conv,out} = \dot{m}_{out} c_{\bar{p},out} T_{out} \tag{24}$$

$$q_{conv,p-plen} = \dot{m}_{in} c_{\bar{p},in} T_{in} \tag{25}$$

$$q_{conv,w-plen} = h_w A_T \left(T_w - T_{plen}\right) \tag{26}$$

The energy balance of the plenum becomes:

$$\dot{m}_{in} c_{\bar{p},in} T_{in} + h_w A_T \left(T_w - T_{plen}\right) - \dot{m}_{out} c_{\bar{p},out} T_{out} = 0 \tag{27}$$

2.3.4 Total energy balance on collector

The heat balance on the collector, illustrated in Fig. 3b, is used to establish the link between the above other three balances considered separately. Performing this global balance, the following expression can be deduced:

$$q_{rad,Sol-w} + q_{rad,Sol-p} - q_{rad,p-amb} + q_{conv,p-amb} - q_{conv,p-loss} - q_{conv,out} - q_{cond,w} = 0 \tag{28}$$

To summarize the different terms involved in the Eq. (28):

$$q_{rad,Sol-w} = \varepsilon_{eff,w} A_T G_{Sol} \tag{29}$$

$$q_{rad,p-amb} = \varepsilon_{eff,p-amb} \tilde{\sigma} A_T \left(T_p^4 - T_{amb}^4\right) \tag{30}$$

$$q_{conv,p-amb} = \dot{m}_{amb} c_{\bar{p},amb} T_{amb} \tag{31}$$

$$q_{rad,out} = \dot{m}_{out} c_{\bar{p},out} T_{out} \tag{32}$$

$$q_{conv,loss} = 0 \tag{33}$$

$$q_{conv,w} = 0 \tag{34}$$

The heat flux $q_{rad,Sol-w}$ is represented as crossing the border of the collector because it is absorbed by the wall.

Thus, the balance all over the collector is written:

$$\left(\alpha_{eff,w} + \alpha_{eff,p}\right) A_T G_{Sol} - \varepsilon_{eff,p-amb} \tilde{\sigma} A_T \left(T_p^4 - T_{amb}^4\right) + \dot{m}_{amb} c_{\bar{p},amb} T_{amb} - \dot{m}_{out} c_{\bar{p},out} T_{out} = 0 \tag{35}$$

The previous relationships allow to determine some performance criteria of the system such as the collector efficiency η, the temperature difference ΔT between the environment and the outlet of the collector and finally the net heat rate recovered q_{out}, using the following expressions:

$$\eta = \frac{\dot{m}_{out} c_{\bar{p},out} T_{out} - \dot{m}_{amb} c_{\bar{p},amb} T_{amb}}{A_T G_{Sol}} \tag{36}$$

$$\Delta T = T_{out} - T_{amb} \tag{37}$$

$$q_{out} = \dot{m}_{out} c_{\bar{p},out} T_{out} - \dot{m}_{amb} c_{\bar{p},amb} T_{amb} \tag{38}$$

2.4 Air properties [9]

The thermophysical properties of air are determined from polynomial curve fits to a data set in [9] for convenience in programming. They are written in the form of $AT^4 + BT^3 + CT^2 + DT + E$ with the constants displayed in Table 1. Air density is obtained with: $\rho = 360.7782T^{-1.00336}$ (kg/m^3).

2.5 Models of the rates of satisfaction

Dimensionless criteria have to be created as the different variables used in this study are not of the same physical units. To solve this problem of scaling, desirability functions to transform the variables into dimensionless criteria have to

Table 1 Properties of air

	A	B	C	D	E
$c_{\bar{p},in}$ (J/kg K)	1.933E−10	−7.999E−07	1.141E−03	−4.489E−01	1.058E+03
ν (m^2/s)	0	−1.156E−14	9.573E−11	3.760E−08	−3.448E−06
K (λ/WK)	0	1.521E−11	−4.857E−08	1.018E−04	−3.933E−04
α_T (m^2/s)	0	0	9.102E−11	8.820E−08	−1.065E−05

Table 2 Levels of criteria

Criteria	Aim	USL	AUC
η	Maximization	20 %	94 %
		ALC	LSL
ΔT	Minimization	10^{-3}K	0.765K
q_{out}	Maximization	180 J	194 J

Table 3 Weight criteria

Criteria	η	ΔT	q_{out}
Weight (%)	50	32	18

be created. But the choice of a desirability function depends on the requirements of the conducted study. In our case, the temperature difference is minimized while the efficiency is maximized, as shown in Table 2. For this purpose, the function of desirability of Harrington is applied [10–12]:
Minimization function:

$$d\left(Y_m\right) = \exp\left(-\exp\left(b_1 + a_1 \cdot Y_m\right)\right), \text{ with}$$
$$a_1 = \frac{\ln\left(\ln\left(0.01\right)/\ln\left(0.99\right)\right)}{AUC - USL},$$
$$b_1 = \ln\left(-\ln\left(0.99\right)\right) - \alpha \cdot USL \quad (39)$$

Maximization function:

$$d\left(Y_m\right) = \exp\left(-\exp\left(\beta + \alpha \cdot Y_m\right)\right), \quad \text{with}$$
$$a_2 = \frac{\ln\left(\ln\left(0.99\right)/\ln\left(0.01\right)\right)}{LSL - ALC},$$
$$b_2 = \ln\left(-\ln\left(0.99\right)\right) - a_2 \cdot LSL \quad (40)$$

Levels of criteria are summarized in Table 2.

Then, the criteria are aggregated according to the aggregation method based on weighted geometric mean of desirability functions [13]. The global desirability function obtained is defined by:

$$OF = \prod_{n=1}^{3} d_n^{w_n}\left(Y_n\right) \quad (41)$$

The weights used are essential because they represent the wishes of the user relating to the implementation of collector. The values of these weights are summarized in Table 3.

2.6 Optimization procedure

The optimization technique used is the systematic scanning approach of design variables (diameter and pitch of the holes) to find the optimal combinations.

In this study, three criteria are considered:

- Minimization of the temperature difference ΔT;
- Maximization of the rate of heat recovered q_{out};
- And maximization of the efficiency of the collector η

The optimization of the modelled multi-objective problem can be summarized as follows:

$$\begin{aligned}
&\text{Find } x = [D, P]^T \\
&\text{Which maximizes} \\
&OF(x) = \{\eta(x), \Delta T(x), q_{out}(x)\} \\
&\text{Subjected to:} \\
&\quad 20\ \% \le \eta\left(x\right) \le 90\ \% \\
&\quad 10^{-3} \le \Delta T \le 0.765 \\
&\quad 180 \le q_{out} \le 194 \\
&\quad 12 \le P \le 24 \\
&\quad 0.8 \le D \le 1.55
\end{aligned} \quad (42)$$

P and D are expressed into mm. For each set of combination of the design variables, the corresponding global objective functions are determined. The candidate solutions obtained are ranked in descending order according to the above corresponding satisfaction criteria.

3 Result and discussions

The study concerned the Cotonou region in the south of Benin. Its geographic coordinates are: latitude 6°22′N, longitude 2°37′E. The sunshine and temperature data used are those recorded during the month of July 2002 in Cotonou, a typical appropriate reference month for the investigation.

Table 4 Physical and geometrical parameters

Parameter	Value
Collector height (m)	10
Collector length (m)	2
Hole pitch (mm)	16
Plate thickness (mm)	2.8
Geometry	Square
Hole diameter (mm)	1.2
Plenum depth (cm)	16
Emissivity of environment	1
Emissivity of plate	0.92
Emissivity of wall	0.92
Reflectivity of plate	0.08
Ambient temperature (°C)	27
Solar radiation (W/m^2)	400

The system of equations have been solved with the simulation software MATLAB, and the desired settings parameters are identified. The numerical results allow to highlight the effect of conception parameters on the characteristics of TTC.

Table 4 summarises the input parameters and the range of their values in the present study. The output parameters estimated were (a) collector efficiency, (b) rate of heat recovered, and temperature difference. The impact of the variation of input data on these parameters are also analysed.

3.1 Performance variation in function of the temperature difference

Generally, energy efficiency is the most suitable factor for predicting the thermal parameters of solar air collectors [14]. It is therefore convenient to study the influence of design parameters on performances. Figure 4 illustrates the typical efficiency curve of the solar collector according to the temperature difference. It can be noted that the efficiency decreases when the temperature difference get larger for a fixed mass flow (here $m_{tot} = 0.014$ kg/s). That means, the collector provides better efficiency when operating at a temperature close to ambient temperature, i.e. for small temperature differences.

3.2 Influence of diameter and pitch of the holes on performance

Increasing the diameter or the pitch of the holes reduces the collector energy efficiency (Figs. 5, 6). These simulation results confirm the experimental data obtained by Badache [5]. The study of the impact of these parameters is necessary to find the optimal combination that maximizes the performance of the TTC.

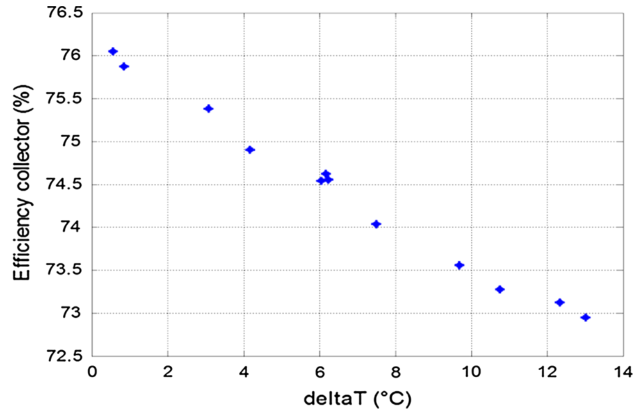

Fig. 4 Variation of collector efficiency versus ($T_{out} - T_{amb}$)

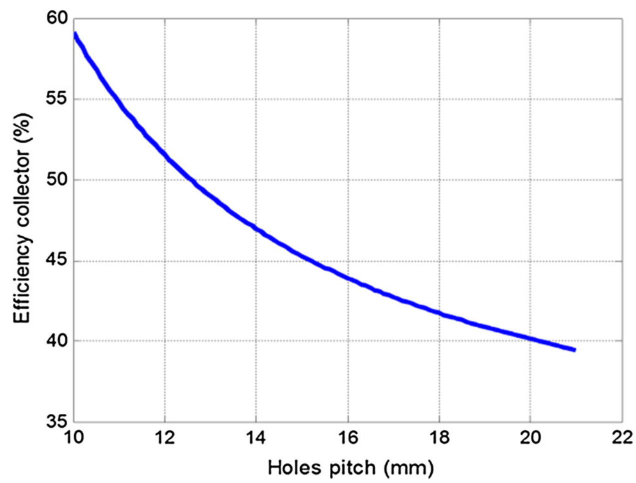

Fig. 5 Variation of collector efficiency with holes pitch

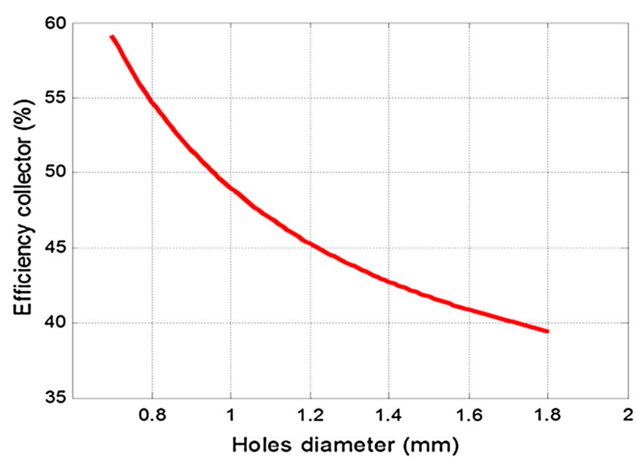

Fig. 6 Variation of collector efficiency with holes diameter

3.3 Effect of holes pitch on the rate of heat recovered

For a constant diameter, the effect of variation in the pitch of the holes on the amount of heat recovered is insignificant.

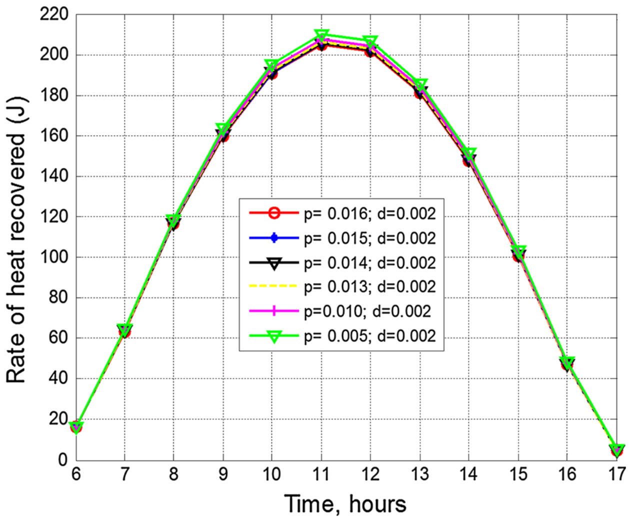

Fig. 7 Variation of the rate of heat recovered as a function of holes pitch

Furthermore, it is mainly between 10 and 13th at the impact of the variation in the pitch of the holes is more significant. Thus, a decrease in pitch of the holes shows a tendency of increase in the amount of heat. This augmentation is due to the fact that a decrease in pitch size of the holes increases the number of holes and therefore, the air flow entering the collector gets considerable.

3.4 Effect of holes diameter on the rate of heat recovered

To a constant pitch, the effect of the variation in the diameter of the holes on the rate of heat recovered is more significant than in the case of Fig. 7. Thus, for a reduction of 1.2 mm of a hole diameter, an increase of 33.71 % has been observed in the energy recovery (Fig. 8) against an increase of 2.43 %, if the pitch size diminishes of 11 mm. The phenomenon observed in Fig. 8 is due to the fact that a reduction of the diameter of the holes causes a reduction in the amount of air entering the plenum, therefore air is preheated quicker.

3.5 Influence of temperature difference on the rate of heat recovered

The trend of the curve in Fig. 8 bmakes it visible that the more the temperature difference increases, the more the heat produced by the collector is low. This phenomenon confirms the trend observed with the performance, i.e. the solar collector is efficient when operating at a temperature close to the ambient.

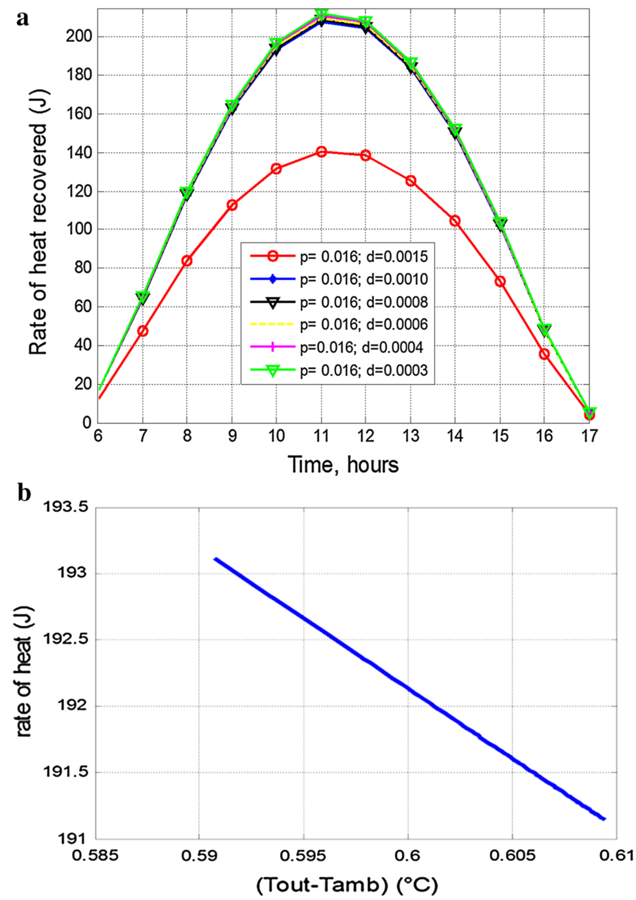

Fig. 8 **a** Amount of Heat recovered vs. diameter and pitch. **b** Variation of heat rate versus ($T_{out} - T_{amb}$)

3.6 Simultaneous impact of the holes diameter and the pitch on the recovered heat rate

Figure 9 shows contours in two dimensions of the rate of heat recovered in function of the diameter and the pitch size of holes. The heat rate is sensitive to the variation of these two parameters. For a given heat rate, an increase in hole diameter induces a need of higher holes pitch to maintain the same amount of energy recovery.

The optimal pair (P, D) to maximize the rate of heat recovery is determined through a graphical research method using both the response surface (Fig. 10) and the response surface contours (Fig. 9). The result gives P = 23 mm and D = 0.7 mm and the maximum value of the corresponding heat rate is $q_{out} = 194.49$J.

3.7 Effect of the combination of the diameter and the pitch of the holes on temperature difference

Figure 11 shows the level curves of temperature difference (ΔT) according to different combinations of diameter and pitch holes. The figure shows that the temperature difference

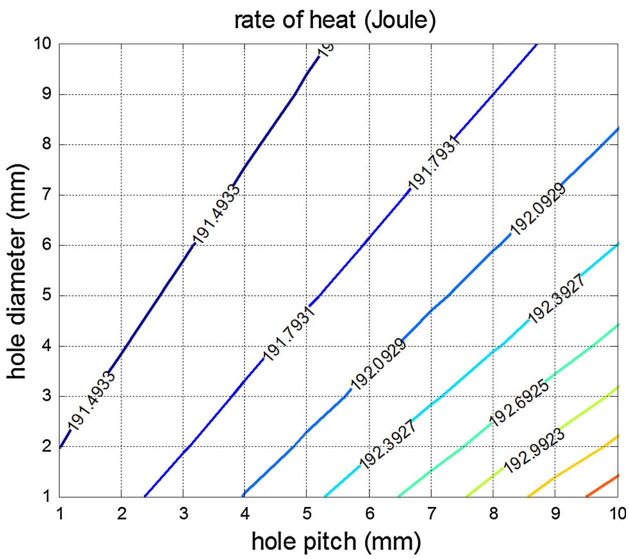

Fig. 9 Rate of heat contours in function of holes diameter and pitch

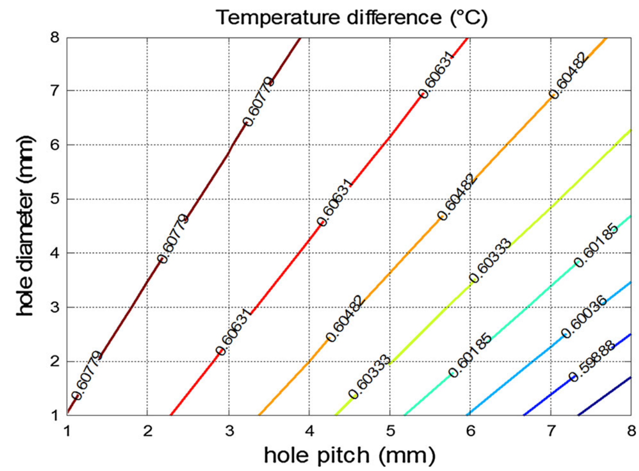

Fig. 11 Temperature difference contours vs. holes diameter and holes pitch

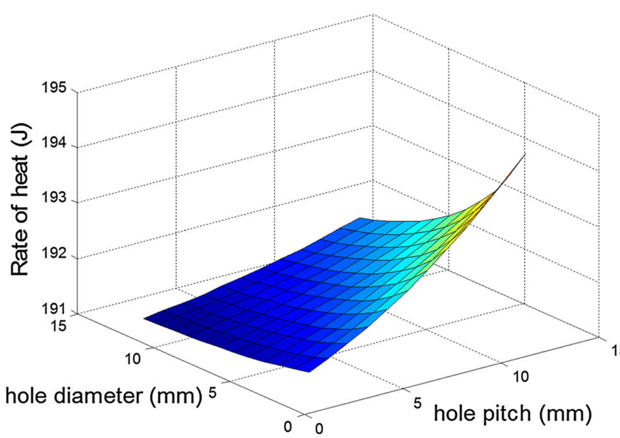

Fig. 10 Response surface of the rate of heat as a function of the holes diameter and pitch

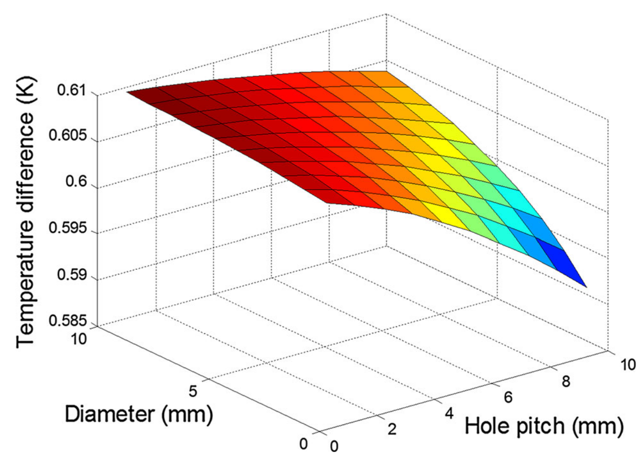

Fig. 12 A 3D representation of ΔT

is relatively insensitive to changes in both design variables. This can be justified by the fact that it is the non-perforated portions of the collector that convert solar radiation into heat. In the range of variation in the diameter and the pitch of the holes, the minimum and maximum values of the temperature difference are respectively 0.5959 and 0.6093 K. The influence appears really weak in value. But a pitch variation of 19–12 mm with an increase in diameter from 0.5 to 1.2 mm generates a 2.2 % decrease temperature.

The optimum pair of design parameters, corresponding to the minimum value of ΔT is: P = 12 mm and D = 1.2 mm. Figure 12 is a 3-D representation of ΔT according to different configurations. Each value of ΔT corresponds to a (P, D) set combination of design variables. Ten values of P and D are examined with respective 1 and 0.1 mm as pitch values. The induced maximum and minimum values of ΔT can clearly be identified.

3.8 Impact of holes diameter and pitch on the performance

In Fig. 13, it can be noticed that the diameter and the holes actually impact the performance η of the collector. But this influence is less pronounced than on the temperature difference. Thus, an increase in pitch of 12–21 mm against a reduction in diameter of 1.4–0.5 mm produces an efficiency increase of the collector of 1.03 %. The corresponding optimal couple (D, P) obtained in diameter and holes pitch is (1.4 mm, 12 mm).

The maximum efficiency that meets these conditions is $\eta = 84.3$ %. Fig. 14 is a 3D representation of the collector energy efficiency according to different configurations. Each value of η corresponds to a set of combination of the design variables (P, D). Ten values of P and D are tested with respective pitches of 1 and 0.1 mm. Maximum and minimum values of η are then identified.

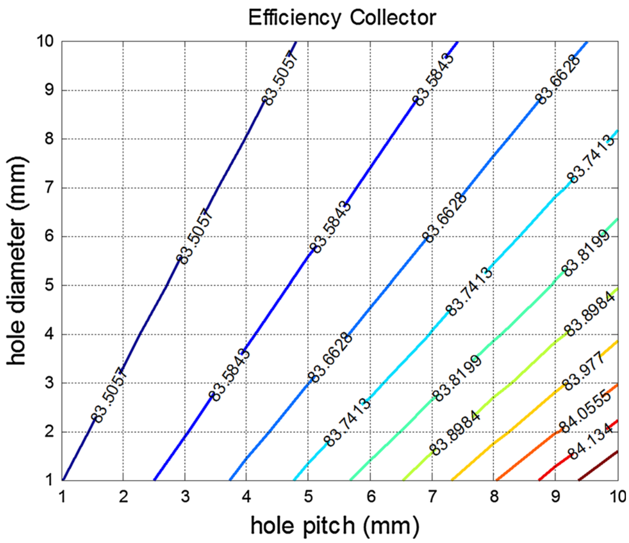

Fig. 13 Efficiency collector contours vs. various holes diameter and holes pitch

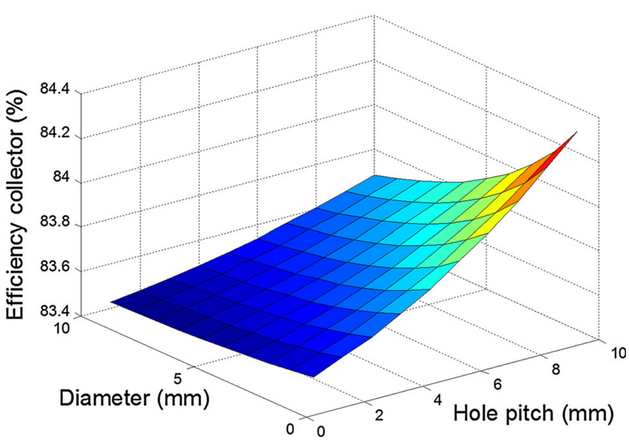

Fig. 14 3 D representation of η

3.9 Optimization based on desirability: optimum holes diameter and pitch

In the previous sections, the optimization of the collector efficiency and the temperature difference was conducted separately in order to determine the (P, D) pairs that maximize the performance η or the recovered heat q_{out} and minimized ΔT.

It was noticed that the optimum pair that maximizes the performance is not the one that maximizes the rate of heat, nor the same that minimizes the temperature difference. We are therefore facing a multi-criteria problem, where the different criteria chosen are contradictory and the search for a compromise is essential. Thus, in this section, we introduce desirability functions to determine the optimal pair of variables (P, D) that minimizes ΔT and simultaneously maximizes q_{out} without degrading the global performance of the collector.

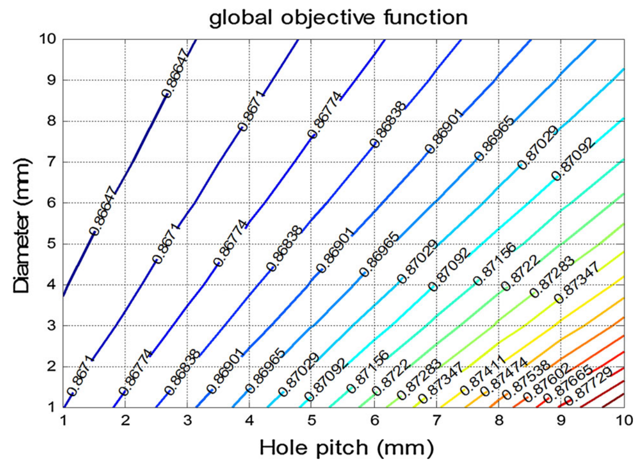

Fig. 15 Contours of global objective function OF

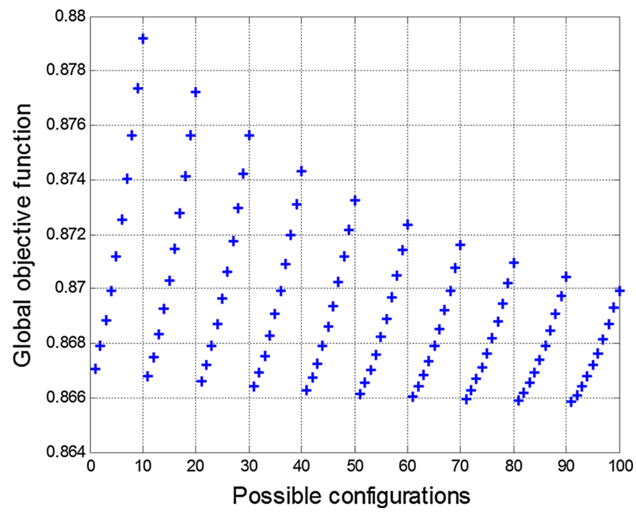

Fig. 16 Evolution of global objective functions vs. possible various configurations

In Fig. 15 are plotted contours of the global objective function with displayed values. The optimal configuration matches with: P $=$ 12 mm, D $=$ 1.4 mm, ΔT $=$ 0.5907 K, $q_{out} = 191.12$J

The Fig. 16 shows all the possible solutions and one sees the best solution, showing the biggest desirability. Table 5 displays the five best solutions with their characteristics. The solutions meet the expectations.

4 Conclusion

In this work a study of the thermal performance of a TTC has been conducted. For the purpose, an analytical model of the physical phenomena that characterize this type of

Table 5 Characteristics of the five best solutions

N°	$P\,(mm)$	$D\,(mm)$	$\eta\,(\%)$	$\Delta T\,(K)$	$q_{out}\,(J)$	OF
1	12	1.4	84.29	0.5907	193.12	0.8517
2	12	1.3	84.16	0.5934	193.83	0.8495
3	13	1.4	84.15	0.5936	192.81	0.8493
4	12	1.2	84.05	0.5959	192.57	0.8474
5	15	1.4	83.96	0.5978	192.37	0.8743

collector has been developed. Simulations are conducted to identify the impact of certain parameters on the performance, the temperature difference and the rate of heat recovered from the collector. The obtained simulation results indicate a good agreement with those obtained experimentally by other researchers. Numerical modelling contributed to a finer understanding of the heat transfer in this new generation of solar collector. The work can help in an optimal design of TTC collectors.

In conclusion, to achieve the goals, we explored different ways to design TTC in compliance with the specifications (solutions with satisfaction requirements). It took implement knowledge of mechanical, industrial and energy engineering. It was also necessary to integrate numerical simulation within collaborative design environments in order to find the best candidate of conception variables. Throughout this approach the goal of this research is reached to reduce risk in decision design, optimize choice in preliminary design and to develop robust design methods.

References

1. Petibon, S.: Nouvelles architectures distribuées de gestion et de conversion de l'énergie pour les applications photovoltaïques. Université Toulouse III, Paul Sabatier, Thèse de doctorat (2009)
2. Petroleum, British.: BP Statistical Review of World Energy (2012). http://www.bp.com/liveassets/bp_internet/globalbp/globalbp_uk_english/reports_and_publications/statistical_energy_review_2011/STAGING/local_assets/pdf/statistical_review_of_world_energy_full_report_2012.pdf
3. Pernet, P.: "Développement de Cellules Solaires en Silicium Amorphe de Type 'n.i.p' surSubstrats Souples". Thèse de l'Ecole Polytechnique Fédérale de Lausanne, 'EPFL', no. 2303 (2000)
4. Semenou, T., Rousse, D.R., Le Lostec, B., Nouanegue, H.F., Paradis, P.L.: Mathematical modeling of dual intake transparent transpired solar collector, Mathematical Problems in Engineering, p. 11. Hindawi Publishing Corporation (2015). doi:10.1155/2015/942854 (Article ID: 942854)
5. Badache, M.: "Etude numérique et expérimentale du transfert de chaleur dans un capteur solaire à perforations doté d'un collecteur transparent et opaque". Thèse de l'Ecole de Technologie Supérieure Université du Québec (2013)
6. Genevès, C.: Modélisation unidimensionnelle d'un collecteur solaire aéraulique. Mémoire de Maîtrise en Génie, Concentration Energies Renouvelables et Efficacité Energétique. Montréal (2013)
7. Kutscher, C.F.: Heat-exchange effectiveness and pressure-drop for air-fow through perforated plates with and without crosswind. J. Heat Transf. Trans. ASME **116**(2), 391–399 (1994)
8. Kutscher, C.F., Christensen, C.B., Barker, G.M.: Unglazed transpired solar collectors - heat-loss theory. J. Solar Energy Eng. Trans. ASME **115**(3), 182–188 (1993)
9. Motahar, S., Alemrajabi, A.A.: An analysis of unglazed transpired solar collectors based on exergetic performance criteria. Int. J. Thermodyn. **13**(4), 153–160 (2010)
10. Sebastian, P., Quirante, T., Ho Kon Tiat, V., Ledoux, Y.: Multi-objective optimization of the design of two-stage flash evaporators: Part 2. Multi-objective optimization. Int. J. Therm. Sci. **49**, 2459–2466 (2010)
11. Wagner, T., Trautmann, H.: Integration of preferences in hypervolume-based multi-objective evolutionary algorithms by means of desirability functions. IEE Trans. Evol. Comput. **14**(5), 688–701 (2010)
12. Semassou, G.C., Guidi, T.C., Dangbédji, C., Degan, G.: Optimal design of a wind system for water pumping using a genetic algorithm. Vestnik Mezhdunarodnoi Akademii Kholoda (2) (2015)
13. Derringer, G.C., Suich, R.: Simultaneous optimization of several response variables. J. Qual. Technol. **12**, 214–219 (1980)
14. Tchinda, R.: A review of the mathematical models for predicting solar air heaters systems. Renew. Sustain. Energy Rev. **13**(8), 1734–1759 (2009)